Proceedings of the 10th IFAC Conference on Foundations of Systems Biology in Engineering, Corfu Island, Greece, September 8-11, 2024

Extending a synthetic Notch morphogen circuit model to construct 2D cell structures

Beyer A. * **Wagner V.** * **Klingel V.** * **Heymann M.** *
Radde N. *,**

* *University of Stuttgart, 70569 Stuttgart, Germany*
** *corresponding author, e-mail: nicole.radde@simtech.uni-stuttgart.de*

Abstract:
Morphogenesis, the process of cells forming a defined shape, is central during embryonic development. Among other cues it involves diffusible signaling molecules, known as morphogens, and concentration-dependent cellular responses to these molecules. Recent advances in synthetic biology have enabled the isolated design and study of cellular systems that mimic morphogenesis. Here, we build on a system from Toda et al. (2020) that uses a synthetic Notch morphogen circuit to trigger and modulate gene expression. Following our vision of a model-based design of different cellular shapes and patterns, we present extensions of this framework based on the current synthetic Notch signaling capabilities described in the literature. We show first results of implementing morphogen-dependent proliferation as a particular example. The proliferation triggered by the morphogen modulates the steepness of the morphogen gradient, which directly translates to the signal readout. Furthermore, our modeling framework allows us to consider and design patterns in 2D that can be modulated by varying the size and location of the morphogen source and those of the interacting molecules, such as morphogen inhibitors. This bottom-up engineering approach opens up opportunities to better understand the underlying principles of morphogenesis and to design complex tissues with desired functions.

Keywords: morphogenesis, synthetic biology, synthetic Notch, partial differential equations

1. INTRODUCTION

Recent developments in synthetic biology promise to enable the modeling-aided design and implementation of building blocks made up of isolated functional modules called synthetic circuits. One of those building blocks is the synthetic Notch (synNotch) platform based on wild-type Notch receptors (Morsut et al., 2016). While wild-type Notch activation requires its ligands to be presented by an adjacent cell (Kopan and Ilagan, 2009), synNotch can be modulated to react upon soluble ligand binding (Smyrlaki et al., 2024).

Wild-type Notch receptors have a large extracellular binding domain for their ligands, proteins of the Delta family, which are presented by opposing cells, and an intracellular transcription regulatory domain that is released upon binding and activates genes that play a role in cell-cell signaling (Kopan and Ilagan, 2009). The synNotch platform introduced by Morsut et al. (2016) retains the Notch core domain, while the ligand-binding and intracellular domains can be freely selected. This allows to build circuits with a customizable sensor, the ligand-binding domain, and a customizable effector, the intracellular domain (Fig. 1A). Toda et al. (2020) introduced synthetic Notch circuits that mimic the behavior of morphogens. Morphogens are long-range signaling molecules that play a vital role during the development of an organism by providing positional information for the individual cells (Wolpert, 1969). They are produced and secreted by one cell type and form a concentration gradient. Other cells respond to the local concentration, which depends on their position relative to the source, by activating different target genes dependent on their own state. This results in multiple areas of cells with different gene expression patterns and is commonly conceptualized by the French flag model, where the three stripes represent three distinct cell fates (Wolpert, 1969). In nature, cells integrate many exterior signals, and cell fate is controlled by the complex interplay and cross-talk mechanisms between these multiple signal transduction pathways. The possibility of developing new synthetic circuits that mimic these processes and artificially add more complexity will help to better understand the biological design principles of morphogenesis.

One particular synNotch circuit is schematically depicted in Fig. 1B. Secretor cells produce and secrete green fluorescent protein (GFP), the morphogen in this context. While unbound GFP diffuses freely, anchor cells can bind and thereby trap unbound GFP. When receiver cells are presented with the GFP-anchor-cell complex, they produce the red fluorescent protein mCherry, visualized by a red-colored cell. Similar to the experimental setting in Toda et al. (2020), a morphogen gradient can be produced by seeding a cell culture well of GFP-secretor cells on one side (the GFP pole) and a mixture of anchor and mCherry-producing receiver cells on the other (the body)

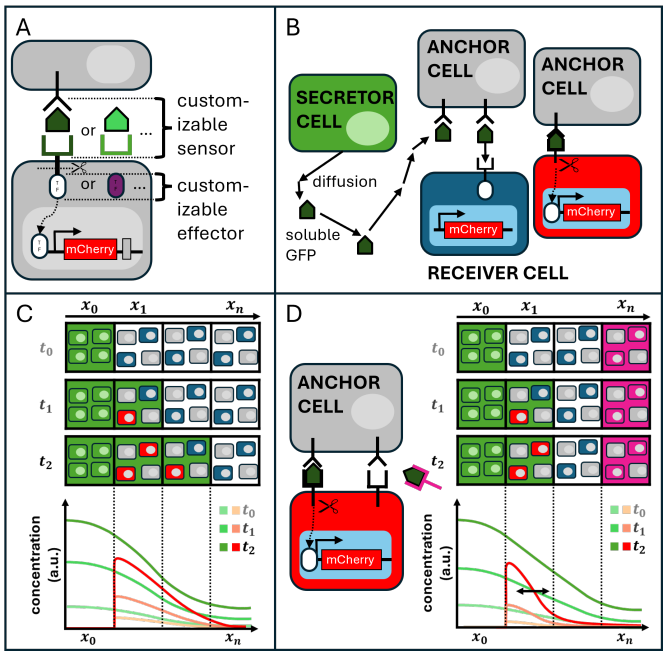

Fig. 1. **The synNotch platform enables synthetic morphogen circuit designs (adapted from Morsut et al. (2016); Toda et al. (2020)).** A: The synNotch platform consists of customizable sensor and effector domains (Morsut et al., 2016). B: One synNotch system from Toda et al. (2020): This synNotch circuit describes a morphogen-like system using a sensor for a green fluorescent protein (GFP) and a transcription activator for a red fluorescent protein (mCherry) as an effector. Receiver cells that sense bound GFP become red. C: Spatial signal readout in the x-direction (1D) at three time points for green GFP and red mCherry signal illustrating similarity to morphogen gradients. Rectangles in the top part illustrate the division of the spatial domain into compartments that are used for the model simulation (Eq. 1). D: System modifications such as adding an inhibitor pole (pink) allow for an amplitude or range shift for both signals (GFP and mCherry) depending on the inhibitor amount and the binding kinetics.

(Fig. 1C). GFP produced in the GFP pole can diffuse into the body, where it is trapped by anchor cells and triggers mCherry expression. The resulting GFP gradient is transferred directly to a gradient in the mCherry expression. If GFP and mCherry are degraded, the system converges to a steady state with gradual GFP concentration and mCherry signal. These gradients can further be shaped by introducing a morphogen inhibitor source, as described by Toda et al. (2020) and indicated in purple in Fig. 1D, resulting in a lower and steeper mCherry signal gradient.

We use the synthetic morphogen system of Toda et al. (2020) as a basis for a flexible *in silico* design with respect to a spatio-temporal distribution of the readout signal and cell proliferation. Therefore, we extend the computational reaction-diffusion model introduced by Toda et al. (2020) in two directions. Firstly, we use synNotch to trigger cell proliferation through the morphogen. A simple Verhulst model is employed for this purpose. Secondly, we expand the design space by extending the model from one dimension to two dimensions. This allows us to generate a wide range of shapes and signals through flexible geometric arrangements of the poles and the body. Together with other design variables such as cell densities and pole sizes, we thus present an *in silico* toolbox for the flexible design of synthetic morphogenesis.

2. RESULTS

Toda et al. (2020) introduced a computational model representing the morphogen circuit depicted in Fig. 1B. It describes the dynamics of four time-dependent chemical species in one spatial dimension: The freely diffusing, unbound morphogen (M), represented by GFP, interacts with an inhibitor (I) with the same diffusion coefficient. In particular, they can bind together, creating the morphogen-inhibitor complex $\hat{I}$. $\hat{M}$ encodes the complex of morphogen and anchor cell and produces a non-diffusing signal represented by the red fluorescent protein (mCherry). The system evolves according to the governing partial differential equations

$$\frac{\partial M}{\partial t} = \underbrace{D\nabla^2 M}_{\text{diffusion}} + \underbrace{k^m_{src} C_M}_{\text{production}} - \underbrace{k_{deg} M}_{\text{degradation}} - \underbrace{k^i_{on} k_\rho M I + k^i_{off} \hat{I}}_{\text{inhibitor binding}} - \underbrace{k^a_{on} k_\rho M(1-\hat{M}) + k^a_{off}\hat{M}}_{\text{anchor binding}} \quad (1a)$$

$$\frac{\partial I}{\partial t} = D\nabla^2 I + k^i_{src} C_I - k_{deg} I - k^i_{on} k_\rho M I + k^i_{off}\hat{I} \quad (1b)$$

$$\frac{\partial \hat{M}}{\partial t} = -k^a_{on} k_\rho M(1-\hat{M}) - k^a_{off}\hat{M} - k_{deg}\hat{M} \quad (1c)$$

$$\frac{\partial \hat{I}}{\partial t} = k^i_{on} k_\rho M I - k^i_{off}\hat{I} - k_{deg}\hat{I} \quad (1d)$$

$$C_M = C_I \in \{0, 1\}, \quad (1e)$$

where D denotes the diffusion coefficient, k^m_{src} and k^i_{src} denote production rates for morphogen and inhibitor, and k_{deg} the degradation rate, which is assumed to be equal for all chemical species. Further, k^i_{on} and k^a_{on} denote the binding rates for the inhibitor (i) and anchor binding (a), k^i_{off} and k^a_{off} define release rates, and k_ρ describes an effective concentration of the anchor cells. Due to limited knowledge about the parameter values, the computational model was designed to be as simple as possible while reproducing the experimental results qualitatively. In Toda's model, the spatial domain is divided into three parts: secreting poles for the morphogen (green compartment on the left in Fig. 1D at t_0) and the inhibitor (pink compartment on the right) at opposing ends and a central body in the middle. For the morphogen- and inhibitor-producing poles only production, diffusion, and degradation are considered. In our representation, this is realized by setting the switch parameter $C_M = 1$ inside the morphogen-producing pole and $C_M = 0$ elsewhere. Similarly, we set $C_I = 1$ inside the inhibitor-producing pole and $C_I = 0$ elsewhere. Binding reactions in the poles are suppressed by setting $k_\rho = 0$. Zero Neumann boundary conditions prevent a flow out of the system boundaries. All concentrations are initialized at zero.

The concentration of anchor-bound morphogen, $\hat{M}$, is the primary readout of this model. It serves as a proxy for the receptor cells' transcriptional response, leading to the production of mCherry. For numerically solving the above

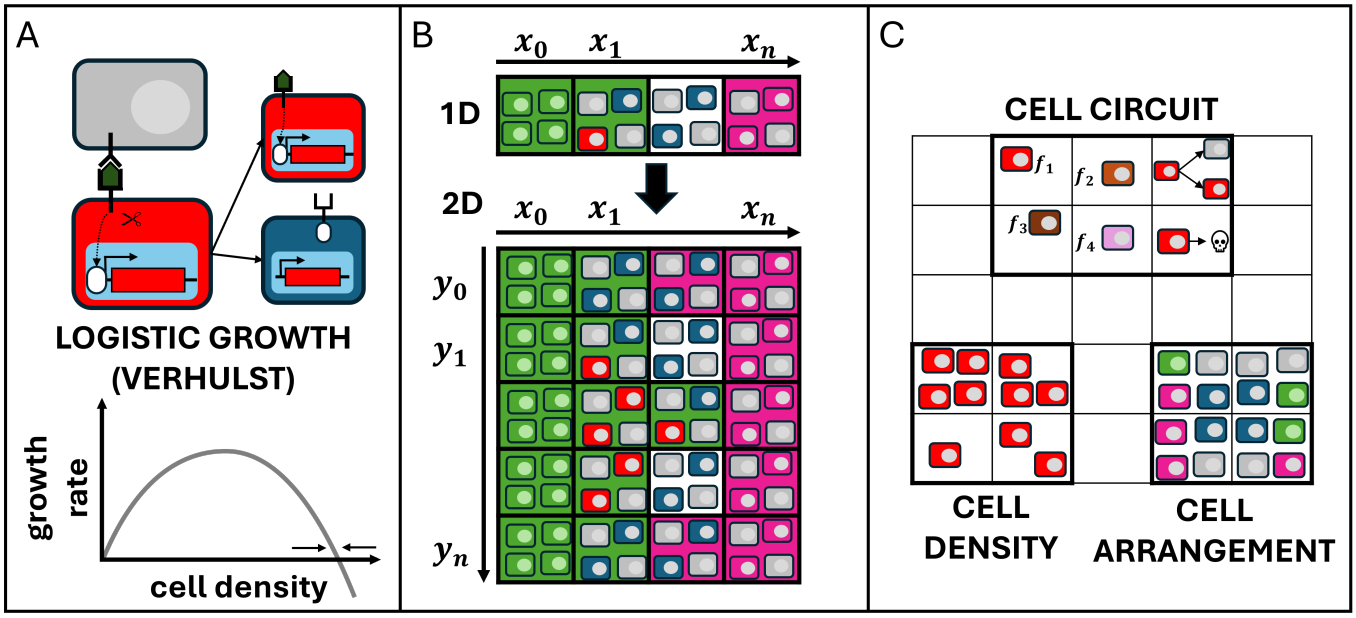

Fig. 2. **Extension of the synNotch platform in Fig. 1**. A: Cells proliferate upon morphogen binding, assuming a maximal cell density following the Verhulst equation for logistic population growth (Eq. 2). B: Moving from a 1D to a 2D model opens up an avenue to design synNotch circuits that exhibit predefined patterns. Rectangles correspond to simulation compartments that are used for numerically solving our model (Eq. 3). C: Design variables include the type of cell circuits that define the overall behavior of single- or multiple-cell interactions, the initial cell numbers, and the arrangement of cells in a 2D space.

system of equations on a computer, its derivatives have to be discretized. To this end, we divide the spatial and temporal dimensions into simulation compartments. We assume all molecules in each compartment are well-mixed. Diffusion occurs as exchange between directly neighbouring compartments following von Neumann neighborhood. The diffusion coefficient is scaled according to the number of simulation compartments. The derivatives are then approximated by finite differences, leading to a solvable system of equations. This well-established approach of discretizing partial differential equations is used throughout this article.

2.1 Model augmentation

We revise and extend Toda's model in four different aspects.

Firstly, our model allows for the diffusion of the morphogen-inhibitor complex $\hat{I}$. Since both the morphogen and the inhibitor diffuse individually, this should not change when they bind to each other.

Secondly, our model enables us to encode different intracellular response circuits triggered by anchor-cell-morphogen complexes. Exemplary, our model couples morphogen binding not only to mCherry production but also to cell proliferation (Fig. 2A). Cell proliferation can be triggered by modulating transcription of pathway proteins that play a role in the cell cycle, e.g. MAPK pathway or the Notch pathway itself (Duronio and Xiong, 2013). Our primary motivation for introducing morphogen-triggered cellular proliferation as the first of our synthetic building blocks is the creation of steeper mCherry expression gradients. The ability to create steep morphogen gradients is interesting, as these gradients allow for the precise triggering of cellular responses. If proliferation is triggered predominantly in compartments with high morphogen concentrations, this further reinforces morphogen binding by increasing the number of available binding sites in these compartments and thus represents a self-reinforcing feedback loop.

To integrate cell proliferation into the model, we explicitly introduce variables that describe the densities of the different cell types. The variables C_M, C_I, C_A, $C_{\hat{M}}$ represent morphogen-producing-, inhibitor-producing-, anchor- and receiver-cells, respectively. As before, we assume anchor- and receiver-cells to be present in equal numbers and therefore set $C_A = C_{\hat{M}}$. Based on the Verhulst equation (Verhulst, 1938), the time-evolution of receiver cells $C_{\hat{M}}$ is described by

$$\frac{\partial C_{\hat{M}}}{\partial t} = \mu \hat{M}\left(1 - \frac{C_{\hat{M}}}{C_{max}}\right), \tag{2}$$

where μ is the proliferation rate and C_{max} is the maximum cell density that is approached logistically. The maximum cell density is motivated by considering the physical size of each simulation compartment and the expected size of the considered cell type. If we consider the experimental scale to be $8^2\,\mathrm{mm}^2$ (Toda et al., 2020) and the area one cell occupies to be $165\,\mu\mathrm{m}^2$ (Milo and Phillips, 1938), then a completely occupied simulation compartment contains about 400 cells. Proliferation is only induced by the morphogen, which is described with a proportionality to $\hat{M}$. We note that Verhulst dynamics also allows for a decrease in cell density, which could be interpreted as cell death, in the case of an over-saturation of $C_{\hat{M}} > C_{max}$. In our model this can only occur when the initial cell seed is higher than the maximum cell density. With the augmentations highlighted in blue, the revised model equations read

$$\frac{\partial M}{\partial t} = \underbrace{D\nabla^2 M}_{\text{diffusion}} + \underbrace{k^m_{src} C_M}_{\text{production}} - \underbrace{k_{deg} M}_{\text{degradation}}$$
$$- \underbrace{k^i_{on} M I + k^i_{off} \hat{I}}_{\text{inhibitor binding}} - \underbrace{k^a_{on} M (C_{\hat{M}} - \hat{M}) + k^a_{off} \hat{M}}_{\text{anchor binding}} \quad (3a)$$

$$\frac{\partial I}{\partial t} = D\nabla^2 I + k^i_{src} C_I - k_{deg} I - k^i_{on} M I + k^i_{off} \hat{I} \quad (3b)$$

$$\frac{\partial \hat{M}}{\partial t} = k^a_{on} M (C_A - \hat{M}) - k^a_{off} \hat{M} - k_{deg} \hat{M} \quad (3c)$$

$$\frac{\partial \hat{I}}{\partial t} = D\nabla^2 \hat{I} + k^i_{on} M I - k^i_{off} \hat{I} - k_{deg} \hat{I} \quad (3d)$$

$$C_M = C_I = \text{const.} \quad (3e)$$

$$\frac{\partial C_{\hat{M}}}{\partial t} = \frac{\partial C_{\hat{M}}}{\partial t} = \mu \hat{M} \left(1 - \frac{C_{\hat{M}}}{C_{max}}\right). \quad (3f)$$

The third and fourth augmentations affect the physical geometry of the simulated reaction system. In particular, our third augmentation extends the spatial domain to two dimensions, as visualized in Fig. 2B. The Laplacian $\nabla^2 M$ in two Cartesian coordinates x and y resolves to $\frac{\partial^2 M}{\partial x^2} + \frac{\partial^2 M}{\partial y^2}$. Further, instead of an effective concentration k_ρ dependent on pole and body regions and the switch parameters C_M and C_I being either zero or one, the reaction rates in our augmented model depend on the cell concentrations (C_M, C_I, C_A, $C_{\hat{M}}$) per simulation compartment. The initial cell concentrations become part of the initial conditions. Concentrations of M, $\hat{M}$ and I are initialized at zero. We also assume zero Neumann boundary and von Neumann neighbouring conditions.

Thus, conceptually, pole and body regions are in this framework solely characterized by the cell type(s) present in the respective simulation compartments rather than by boolean variables. The spatial modeling flexibility achieved by combining all our model augmentations is demonstrated in Fig. 2C and includes different cellular responses via different circuits, variations in cell densities, and different cell arrangements.

2.2 The augmented model reproduces the experimental data

The changes made in the model, in particular, the coupling of production rates to cell densities, require an adjustment of the model parameters so that the augmented model reproduces the experimental data just as well as the original model. This was already easily achieved by manual adjustment, and all parameter values used for this article's simulation results are reported in Appendix A. A comparison of our simulation with the experimental data from Toda et al. (2020) is depicted in Fig. 3A, demonstrating that our model is indeed capable of reproducing the experimental data.

By adding an inhibitor pole to the right end of the simulation domain, the model produces a steeper mCherry expression gradient (Fig. 3B). At the same time, the overall signal readout is lowered as a fraction of the morphogen M is sequestered by the inhibitor I, forming a complex $\hat{I}$. Since this diffusing complex $\hat{I}$ can also dissociate back into its parts, the morphogen gradient M is flatter and more

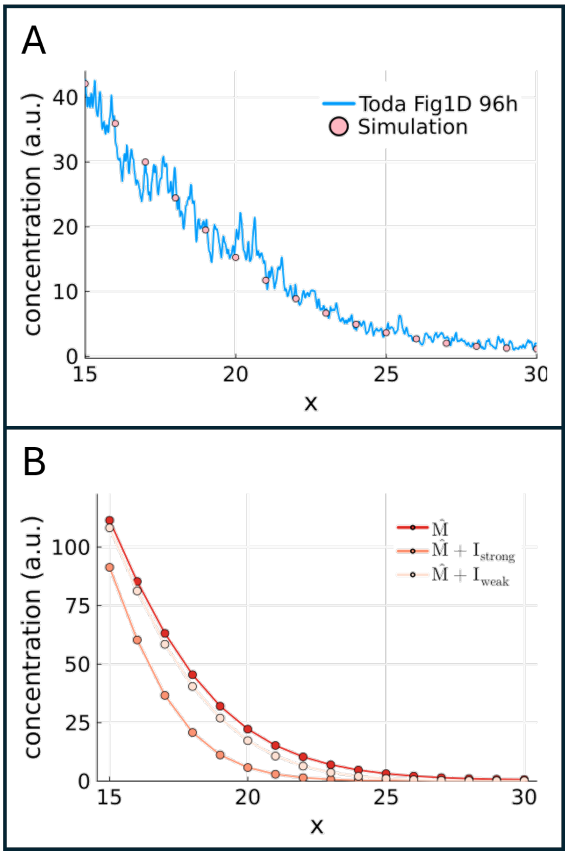

Fig. 3. **The augmented model reproduces the experimental results.** A: Augmented simulation model without proliferation ($\mu = 0$) vs. experimental results presented by Toda et al. (2020) in their Figure 1D. As the experimental readout is an arbitrary fluorescence intensity for the mCherry signal, the simulation output was normalized at $x = 0$ to the experimental data. B: The addition of an inhibitor pole at x_{end} results in a steeper gradient and shifts mCherry ($\hat{M}$) readout away from the inhibitor pole. The shift is more pronounced with a strong inhibitor binding rate ($k^i_{on} = 6 \cdot 10^{-4}$) compared to a weak inhibitor binding rate ($k^i_{on} = 6 \cdot 10^{-5}$). Individual dots represent the value of one simulation compartment.

diluted than with a non-diffusing complex. The steepness of the mCherry gradient is influenced by the inhibitor rates k^i_{on} and k^i_{off}. A smaller k^i_{on} shifts the gradient slightly away from the inhibitor source while a stronger inhibitor gives a more pronounced shift (Fig. 3B).

Summarizing, our augmented model is able to reproduce the experimental findings from Toda et al. (2020).

2.3 Addition of a proliferation function to the circuit allows for steeper gradients and amplifies the readout signal

After successfully reproducing the original model prediction, we harness the extended capabilities of the augmented model. The time-evolution of the readout, mCherry, in one spatial direction x for an early (t_{start}), intermediate (t_{mid}) and late (t_{end}) time-point of the simulation with and without cellular proliferation are compared

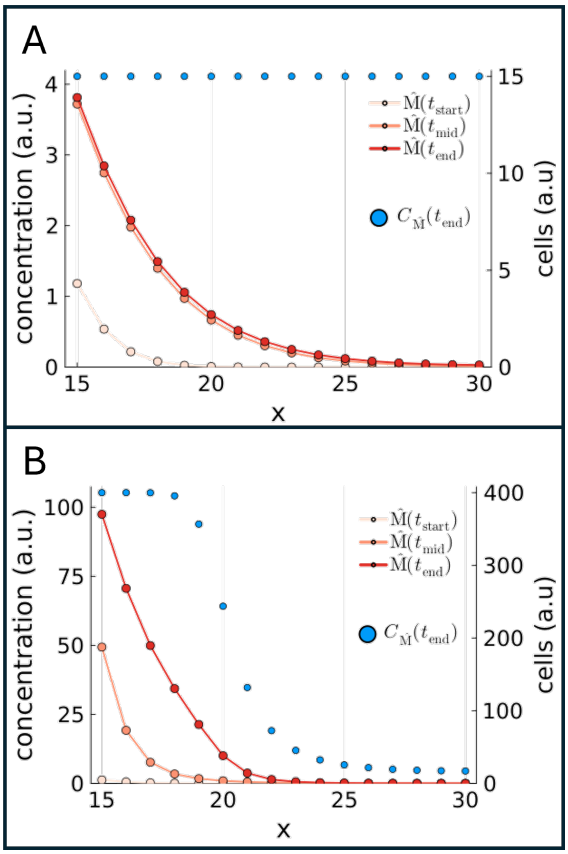

Fig. 4. **Morphogen-triggered proliferation amplifies the signal and results in a steeper gradient.** A: Morphogen M and trapped morphogen $\hat{M}$ gradients at an early (t_{start}), intermediate (t_{mid}) and late (t_{end}) time-point of the simulation for a constant cell density. B: Morphogen M and trapped morphogen $\hat{M}$ gradients with $\hat{M}$-dependent logistic proliferation leads to $\hat{M}$ signal amplification and a steeper gradient.

in Fig. 4. More specifically, one simulation keeps a constant anchor density of 15 cells per compartment (Fig. 4A), while in another simulation anchor cells were allowed to proliferate from an initial density of 15 cells per compartment following our proliferation function (Fig. 4B). As expected, the simulation including proliferation strongly amplifies the mCherry signal. Moreover, it produces a much steeper mCherry expression gradient, especially close to the morphogen source on the left of the spatial domain, as the anchor density and, thereby, the concentration of possible binding sites locally increases (Fig. 4B). This demonstrates that using this cellular proliferation model building block is convenient to achieve steep, nearly switch-like gradients.

2.4 Towards modeling morphogenesis: Higher dimensions and involved geometries

So far, we considered only 1D simulation domains. However, morphogenesis is particularly interesting in higher dimensions, as the cells can form a wide variety of different patterns. Accordingly, our 2D simulations concentrate on dynamics where cell seeds can be placed arbitrarily in space. Finding suitable parameters to form a defined shape in 2D is non-trivial and will also heavily depend on the chosen initial conditions. The initial spatial cell seed for

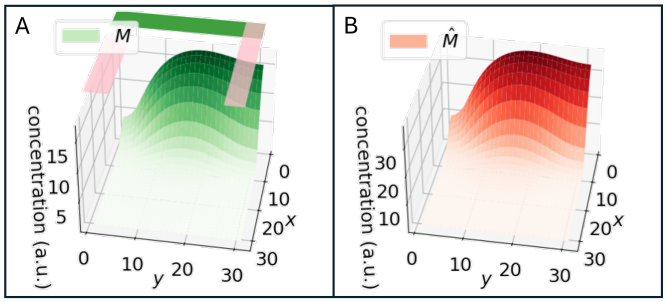

Fig. 5. **Exemplary simulation of the fully augmented model in 2D.** A: Initial conditions are plotted as blocks hovering over the surface plot. Green regions correspond to compartments with morphogen-secreting cells, purple areas encode inhibitor-secreting cells. Both secreting cell types are present in the top-right corner. The surface plot shows the morphogen gradient at the end of the simulation. B: Signal readout, mCherry gradient.

the 2D simulation results depicted in Fig. 5 is indicated by the purple and green areas above the coordinate system. The surface plots show the morphogen M and mCherry $\hat{M}$ gradients in 2D at the end of the simulation. We were able to generate steep gradients in two dimensions and a non-trivial pattern of mCherry expression that forms directionally.

3. DISCUSSION & CONCLUSION

Advances in synthetic biology promise to enhance our understanding of biochemical processes and allow for their precise manipulation. Supported by sophisticated simulation models, these advances can be achieved faster and cheaper.

The established model introduced by Toda et al. (2020) describes a synthetic Notch circuit that mimics the behavior of morphogens. Here, we have proposed a versatile extension of their model. While the original model mainly reports morphogen binding to receptor cells, our model can encode an actual cellular response triggered by morphogen exposure. As an exemplary building block, the morphogen modeled in this paper triggers proliferation, which is limited by the available space for an individual cell. Our simulation results suggest that a circuit with a morphogen-initiated proliferation response creates a steep morphogen and mCherry gradient and thus has a similar effect as adding an inhibitor, as realized in Toda et al. (2020).

In addition, our framework also offers great flexibility in designing a heterogeneous 2D physical domain in which different cell types interact to form complex patterns. This enables the study of complex 2D geometries resembling biological geometries of interest or entirely new ones.

Our vision of designing synthetic systems that mimic specific features of morphogenesis *in silico* is a challenging inverse problem. First, from a modeling perspective, this involves tailored experiments and calibration of the model to experimental data, which is itself a computational challenge (Wagner et al., 2024), as well as validation of the model's predictive capabilities. Second, the design space

including geometric arrangements and circuit tuning must be adapted to the experimental possibilities and carefully defined in order to be able to solve the design problem from a computational point of view.

We already outlined many interesting aspects of our augmented model. However, it is only a first step, paving the way for future research. For example, we have to consider an exchange of cells between simulation compartments due to overgrowth or detachment and reattachment after maximum cell density is reached, which contributes to effective directed growth rates. Also the simplifying assumptions that the densities of the anchor and the receiver cells are equal and that the mCherry signal directly reflects bound morphogen limit our system. Functionally decoupling these cell types as well as considering further sensory receptor systems (Manhas et al., 2022) and intermediately produced species will allow for even more complex patterns. Our goal is to harness the ability to iteratively add further functional modules related to morphogenesis such as an ultrasensitive transcriptional response to the morphogen gradient (Cotterell and Sharpe, 2010) or varying degradation and diffusion rates (Shilo and Barkai, 2017). This will hopefully aid in the design of more complex patterns and understanding of morphogen signaling during embryonic development from the bottom up.

In conclusion, the extended modeling framework presented in this work outlines and highlights the possibilities of sophisticated simulation models in the context of synthetic biology and, more precisely, morphogenesis. At the same time, further model facets are imaginable, and we are curious to test the chances, challenges, and limits in different future research avenues opened by this work.

ACKNOWLEDGEMENTS

Funded by Deutsche Forschungsgemeinschaft (DFG, German Research Foundation) under Germany's Excellence Strategy - EXC 2075 – 390740016. We acknowledge the support by the Stuttgart Center for Simulation Science (SimTech) and by the state of Baden-Württemberg through bwHPC.

4. IMPLEMENTATION AND CODE AVAILABILITY

All simulation results presented herein are implemented in Julia (Bezanson et al., 2017) and can be accessed through our FAIRDOM Hub repository (https://fairdomhub.org/studies/1259). We used our own finite differences implementation to discretize all derivatives over equidistant grids of $N_x = 31$ compartments in 1D and $N_x \cdot N_y = 31^2 = 961$ compartments in 2D. Simulation parameters are reported in Appendix A.

REFERENCES

Bezanson, J., Edelman, A., Karpinski, S., and Shah, V.B. (2017). Julia: A fresh approach to numerical computing. SIAM review, 59(1), 65–98. doi:10.1137/141000671.

Cotterell, J. and Sharpe, J. (2010). An atlas of gene regulatory networks reveals multiple three-gene mechanisms for interpreting morphogen gradients. Molecular Systems Biology, 6(1), 425. doi:10.1038/msb.2010.74.

Duronio, R.J. and Xiong, Y. (2013). Signaling Pathways that Control Cell Proliferation. Cold Spring Harbor Perspectives in Biology, 5(3), a008904–a008904. doi:10.1101/cshperspect.a008904.

Kopan, R. and Ilagan, M.X.G. (2009). The Canonical Notch Signaling Pathway: Unfolding the Activation Mechanism. Cell, 137(2), 216–233. doi:10.1016/j.cell.2009.03.045.

Manhas, J., Edelstein, H.I., Leonard, J.N., and Morsut, L. (2022). The evolution of synthetic receptor systems. Nature Chemical Biology, 18(3), 244–255. doi:10.1038/s41589-021-00926-z.

Milo, R. and Phillips, R. (1938). Cell Biology by the Numbers. Garland Science. doi:10.1201/9780429258770.

Morsut, L., Roybal, K.T., Xiong, X., Gordley, R.M., Coyle, S.M., Thomson, M., and Lim, W.A. (2016). Engineering Customized Cell Sensing and Response Behaviors Using Synthetic Notch Receptors. Cell, 164(4), 780–791. doi:10.1016/j.cell.2016.01.012.

Shilo, B.Z. and Barkai, N. (2017). Buffering global variability of morphogen gradients. Developmental Cell, 40(5), 429–438. doi:10.1016/j.devcel.2016.12.012.

Smyrlaki, I., Fördős, F., Rocamonde-Lago, I., Wang, Y., Shen, B., Lentini, A., Luca, V.C., Reinius, B., Teixeira, A.I., and Högberg, B. (2024). Soluble and multivalent Jag1 DNA origami nanopatterns activate Notch without pulling force. Nature Communications, 15(1), 465. doi:10.1038/s41467-023-44059-4.

Toda, S., McKeithan, W.L., Hakkinen, T.J., Lopez, P., Klein, O.D., and Lim, W.A. (2020). Engineering synthetic morphogen systems that can program multicellular patterning. Science, 370(6514), 327–331. doi:10.1126/science.abc0033.

Verhulst, P. (1938). Notice sur la loi que la population poursuit dans son accroissement. Correspondance Mathématique et Physique, 10, 113–121.

Wagner, V., Castellaz, B., Kaiser, L., Höpfl, S., and Radde, N. (2024). Eulerian parameter inference: A probabilistic change of variables for model-based inference with high-variability data sets. doi:10.21203/rs.3.rs-4003283/v1.

Wolpert, L. (1969). Positional information and the spatial pattern of cellular differentiation. Journal of Theoretical Biology, 25(1), 1–47. doi:10.1016/S0022-5193(69)80016-0.

Appendix A. PARAMETER VALUES

Parameter	Fig. 3A	Fig. 4	Fig. 5
k^m_{src}	0.09	0.09	0.057
k^i_{src}	0.06	0.06	0.06
k^i_{on}	0.0	0.0	0.7
k^i_{off}	0.0	0.0	0.5
t_{max}	960	960	960
C_{max}	400	400	400
μ	0	0.1	2.0
N_x	31	31	31
N_y	31	31	31
k^a_{on}	0.0006	0.0006	0.006
k^a_{off}	0.9999	0.9999	0.9999
k_{deg}	0.02	0.02	0.02
D	0.02	0.02	0.1